CONFERENCE PRE-PRINT

STELLARATOR PLASMA START-UP MODEL BASED ON ENERGY CONFINEMENT TIME SCALING LAWS, EXPERIMENTAL VERIFICATION AND NUMERICAL SIMULATION RESULTS

Chunyan Li ¹, Pingwei Zheng ^{1,2,*}, Xinchen Jiang ^{3,4}, Xueyu Gong ^{1,*}, Zhengkun Gao ¹

- ¹ School of Nuclear Science and Technology, University of South China, Hengyang, Hunan Province, PR China
- ² School of Resource Environment and Safety Engineering, University of South China, Hengyang, Hunan Province, PR China
- ³ ENN Science and Technology Development Co., Ltd., Langfang, P.R. China
- ⁴ East China University of Science and Technology, Shanghai, P.R. China

E-mail: pwzheng@usc.edu.cn and gongxueyu@126.com

Abstract

Based on the energy confinement time scaling law of stellarator in the low-confinement mode, combined with energy balance equation and the plasma propagation and power deposition equations of the electron cyclotron wave in the three-dimensional magnetic field, a stellarator plasma start-up model including electron cyclotron resonance heating (ECRH) and impurity radiation power loss is established. Validation against W7-X experimental data demonstrates good agreement in the temporal evolution of electron temperature and radiation losses, which verified that the model can correctly give the plasma start-up results of the stellarator under ECRH. This model is applied to predict the results of plasma start-up under 28 GHz ECRH for China Helical Device 1 (CN-H1) stellarator. The effects of the ion-to-electron temperature ratio (T_i/T_e), ECRH injection power (P₀), deposition position, and impurity concentrations (iron) on start-up are systematically studied and analyzed. Results show that increasing T_i/T_e enhances the flat-top electron temperature, which indicates that the increase of ion temperature will help the electron temperature to reach a higher level. Higher P₀ accelerates electron temperature rise and increases flat-top electron temperature, radiative losses decrease notably when P₀ > 200 kW. When the power is deposited on the low-field side and moves from the far-axis to the on-axis region, the rising rate of the electron temperature and the flat-top electron temperature increase accordingly. In addition, the concentration of iron impurity should be less than 0.8% to ensure the effective starting and heating of the plasma. Under optimal conditions ($T_i/T_e = 1$, $P_0 = 200$ kW, central deposition, 0.1% Fe), the ECRH power absorption efficiency is rapidly increased to 94.8%. At a density of 2×10^{18} m⁻³, the electron temperature can reach 373.3 eV and the impurity line radiation power peak is 1.1 kW.

1. INTRODUCTION

Stellarators are regarded as a key candidate for fusion reactor designs due to their potential for steady-state operation and the absence of plasma current drive requirements [1]. Compared with the tokamak, the stellarator does not have a central solenoid design, thus lacking Ohmic heating. Instead, stellarators require RF wave heating to generate high-temperature, high-density plasma [2]. University of South China has introduced the H1-NF stellarator [3-44] from the Australian National University and is currently restoring and reconstructing it into the China Helical Device 1 (CN-H1) stellarator [5-66]. The CN-H1 is a three-period medium-sized stellarator with a main radius of R = 1.0 m, an average small radius of R = 0.2 m, and a maximum designed magnetic field up to 1.0 T. At low magnetic fields (less

than 0.25 T), the CN-H1 stellarator operates in a steady-state mode, and at higher magnetic fields it operates in a pulse mode.

In the electron cyclotron frequency band, the CN-H1 stellarator is planned to use 2.45 GHz microwave and 28 GHz electron cyclotron heating to initiate and maintain the plasma. Liu Yizhuo *et al.* [7] developed a 0D ECRH start-up model for CN-H1 stellarator based on physical model of tokamak start-up. Their results showed that electron density obtained by start-up can reach the order of 10^{17} - 10^{18} m⁻³ by 28 GHz ECRH start-up. However, this model does not consider the effect of the magnetic field configuration of the stellarator and the energy deposition position of the EC wave in the start-up process.

Using the τ_{97L} energy confinement scaling law for tokamaks, Masayuki Ono established a fundamental-mode non-inductive current start-up model for electron cyclotron wave in the spherical tokamak magnetic field configuration. This model was applied to the SHPD Tokamak Facility and the STAR device [8]-11]. In this model, the EC power absorption (P_{ECH}) is calculated using the ray tracing code RT-4 [12]. Compared to other start-up models, this model can better consider the influence of magnetic field configuration and EC wave energy deposition position on the starting process.

On this basis, this study modified the model proposed by Masayuki Ono to be more suitable for the plasma start-up of the stellarator, where plasma current is not required to generate closed magnetic flux surfaces during start-up. In this paper, based on the energy confinement time scaling law of the low-confinement mode (L mode) of the stellarator, combined with the energy balance equation, the plasma propagation equation and the power deposition equation of the electron cyclotron wave in the three-dimensional (3D) magnetic field, a plasma start-up model suitable for the stellarator is established. In order to verify the reliability of the model, the start-up results of the W7-X stellarator [13]-14] simulated by the model are compared with the experimental results under the same plasma condition parameters, and the results are in good agreement. In this paper, the model is further used to study the EC wave start-up at 28 GHz for CN-H1 stellarator. The effects of the ion-to-electron temperature ratio, ECRH injection power, power deposition location, and typical impurity concentrations (iron) are systematically analyzed to assess their impact on the start-up process.

2. THEORETICAL MODELING OF STELLARATOR START-UP

In our stellarator start-up model, the ray trajectory of the EC wave and the corresponding absorbed power from ECRH are calculated using the equations governing EC wave propagation and power deposition in a three-dimensional magnetic field. The electron temperature T_e and the normalized beta β are then used to compute the plasma energy confinement time. Based on the τ_{04L} energy

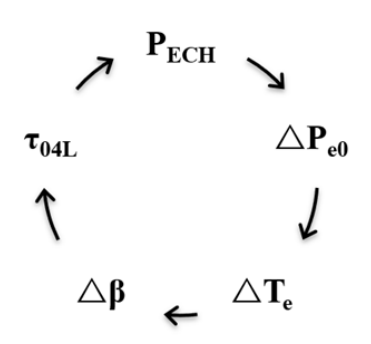


FIG.1 Stellarator plasma start-up model.

confinement scaling law and the absorbed power P_{ECH} , the updated electron plasma pressure is obtained. Since the plasma density is pre-specified, a new electron temperature can be derived. With this updated temperature, a new ray tracing calculation is performed to obtain updated values of τ_{04L} and P_{ECH} . This iterative process forms a feedback loop, as shown in Figure 1.

3. MODEL VALIDATION

To ensure the validity and reliability of the established model in practical applications, simulations of

the plasma start-up process in the W7-X stellarator were conducted. Two scenarios were considered, corresponding to injected powers P_0 of 2.7 MW and 5 MW, respectively. Based on experimental start-up data from W7-X 错误!未找到引用源。, the simulation parameters were set as follows: the effective charge number Z_{eff} was 1.5; the wave injection position was specified by coordinates $(R_i, \varphi, Z_i) = (6.55 \text{ m}, -6.567^{\circ}, -0.1 \text{ m})$ m), where R denotes the radial distance from the EC wave injection port to the machine axis, φ represents the toroidal angle along the stellarator geometry, and Z is the vertical position relative to the midplane, $f_{ec} = 140$ GHz, corresponding to a resonance magnetic field $B_{res} = 2.5 \text{ T}$. The initial electron temperature and density were assumed to be 0.3 keV and 3×10^{18} m⁻³, respectively. The injected wave mode was X2.

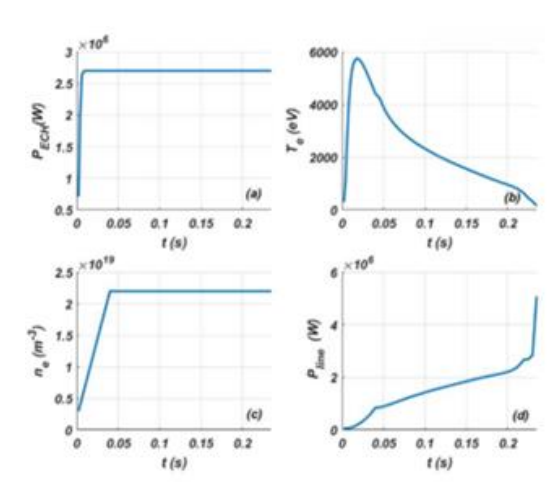


Fig. 2 $P_0 = 2.7$ MW, Temporal evolution of (a) ECRH power absorption, (b) electron density, (c) electron temperature and (d) radiation power with time.

Figure 2 shows the simulation results by our model under 2.7 MW ECRH power injection. As the electron density increases from 3×10^{18} m⁻³ to 2.2×10^{19} m⁻³, the electron temperature initially rises and approaches approximately 6 keV. However, with the gradual increase of radiative power losses, the electron temperature begins to decline. Once the P_{line} exceeds the absorbed ECH power P_{ECH} , the electron temperature T_e drops below 2 keV. This evolution is consistent with the experimental observations from W7-X.

Figure 3 shows the simulation results for a higher ECRH injection power of 5 MW. As the electron

density increases, the computed electron temperature exceeds 4 keV, which is in good experimental agreement with measurements. Although some discrepancies are observed in the absolute values of the radiated power, the magnitude remains on the order of megawatts in both simulation and experiment. This indicates that the model reliably captures the trends in electron temperature evolution and provides a reasonable estimation of radiative power under given density and power conditions. Possible sources of the discrepancies in radiative power include: enhanced absorption efficiency due to optimized injection geometry; measurement uncertainties in experimental diagnostics of radiated power and deviations introduced by interpolation of atomic data from the ADAS database used in the numerical simulations.

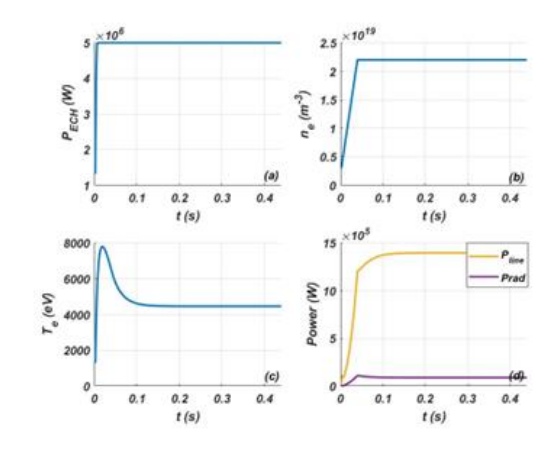


FIG. 3 $P_0 = 5$ MW, Temporal evolution of (a) ECRH power absorption, (b) electron density, (c) electron temperature and (d) radiation power and diffusive power with time.

4. RESULTS OF CN-H1 PLASMA START-UP

The start-up of the CN-H1 stellarator using ECRH was simulated in this study. The initial conditions for the CN-H1 stellarator were set as follows: the injected power P_0 was 200 kW, the effective charge number Z_{eff} was 2, and the wave injection position was $(R_i, \varphi, Z_i) = (1.40 \text{ m}, 15^\circ, -0.1 \text{ m})$. The ECRH frequency was $f_{ec} = 28 \text{ GHz}$, corresponding to a resonance magnetic field $B_{res} = 0.5 \text{ T}$. The initial electron temperature and density were assumed to be 0.03 keV and $1 \times 10^{17} \, \text{m}^{-3}$. The injected wave mode was the X2. Iron impurity radiation was considered due to the material composition of internal components.

4.1 Effect ion-electron temperature ratio (T_i/T_e) on start-up

During the start-up phase, a significant disparity often exists between the electron temperature Te and the

ion temperature T_i . In this section, the results of the influence of different T_i/T_e ratios $(T_i/T_e = \alpha)$ on CN-H1 plasma start-up are given.

Figure 4 shows the effect of different α values on ECRH power absorption during the start-up process. As the proportion of ion temperature increases, the proportion of electron temperature in α is relatively reduced, and the power absorption of ECRH is improved slightly, but this process is 4accompanied by a delay phenomenon. The P_{ECH} was 184.6 kW for $\alpha = 0.5$, 189.6 kW for $\alpha = 1$, and 190.2 kW for $\alpha = 1.5$. Although the increase of ion temperature resulted in a larger P_{ECH} and a delayed

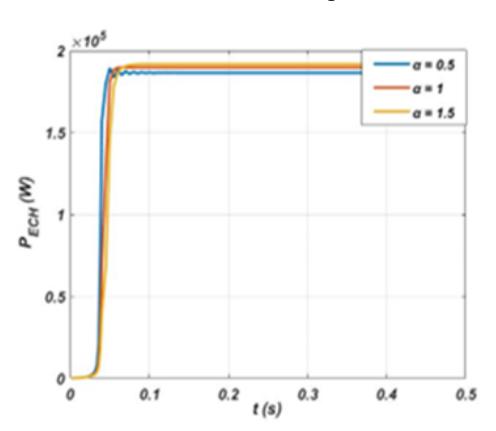


FIG. 4 The effect of α on power absorption.

rise, the amplitude of the changes was relatively small, indicating that the change of ion temperature did not have a significant effect on the power absorption of the EC wave.

As shown in Figure 5, a higher α delays the temperature rise but yields a higher flat-top electron temperature, achieving 325.2 eV, 373 eV, and 425.5 eV for α = 0.5, 1, and 1.5, respectively. These findings indicate that enhancing the initial ion temperature can facilitate higher electron temperatures during the plasma start-up, thereby improving overall heating efficiency.

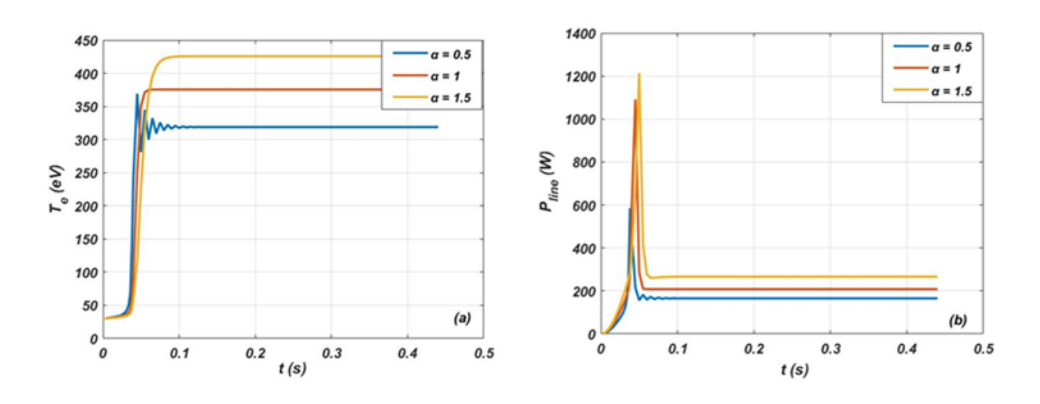


FIG. 5 The effect of α on (a) the electron temperature and (b) the line radiation power.

4.2 Effect of injection power on start-up

The influence of injected power (P_0) on the plasma start-up was investigated for different ion-to-electron temperature ratios ($\alpha = 0.5$, 1). As shown in figure 6, for both α values, a higher injected power leads to a higher final electron temperature. A characteristic initial dip in temperature is observed at lower power levels ($P_0 < 200 \text{ kW}$) before the temperature rises, a trend that diminishes as power increases.

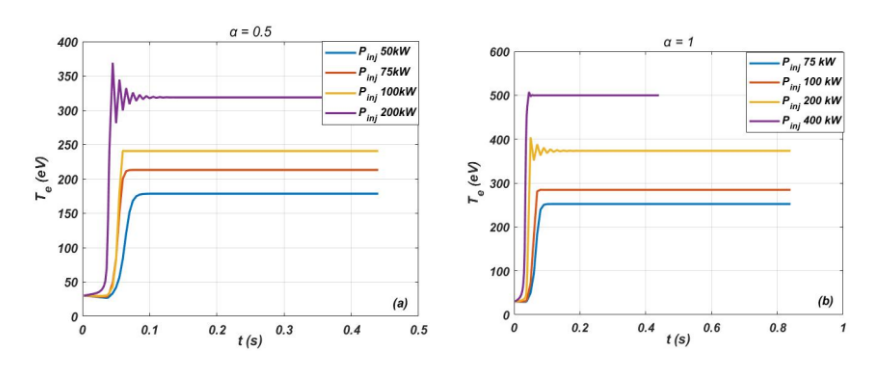


FIG. 6 Effect of injection power on electron temperature. (a) $\alpha = 0.5$ (b) $\alpha = 1$

As shown in Figs. 7 and 8, the EC wave absorption efficiency increases with injected power for both α values, exceeding 94% at $P_0 \ge 200$ kW. A key finding is that for $\alpha = 1$, higher power (400 kW) reduces the peak line radiation power, as the resulting higher electron temperature decreases the population of excited states available for radiative transitions. This demonstrates that increased power can mitigate line radiation losses. Based on these results, $\alpha = 1$ is selected for subsequent simulations to simplify the analysis.

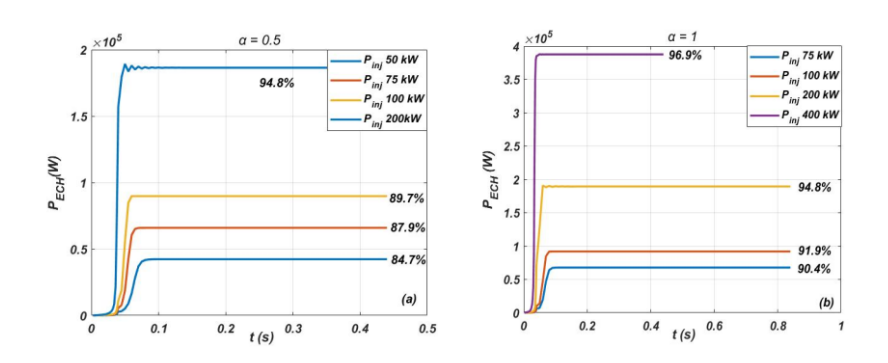


FIG. 7 Effect of injected power on power absorption. (a) $\alpha = 0.5$ (b) $\alpha = 1$

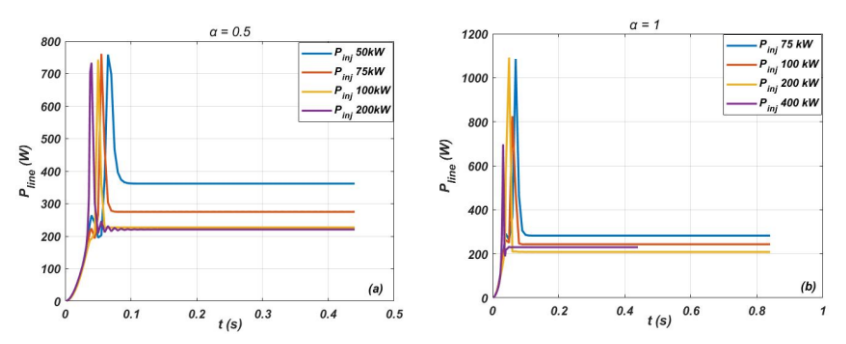


FIG.8 Effect of injected power on line radiation power. (a) $\alpha = 0.5$ (b) $\alpha = 1$

4.3 Effect of ECRH power deposition position on start-up

The impact of ECRH power deposition location was evaluated by scanning four normalized radial positions: low-field side (LFS) off-axis ($\rho = 0.7$), LFS near-axis ($\rho = 0.1$), on-axis, and high-field side (HFS) off-axis ($\rho = 0.3$).

Figure 9 shows that EC wave power absorption is strongly dependent on deposition location, increasing from 85 kW to 189.6 kW as heating shifts from low-field side (LFS) off-axis (ρ =0.7) to the plasma core. This is due to enhanced wave damping from higher magnetic field strength and electron density in central regions. Notably, while high-field side (HFS) off-axis heating (ρ =0.3)

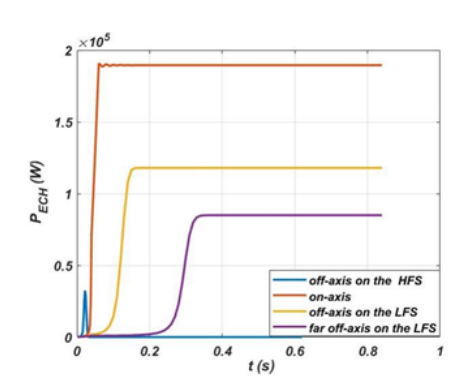
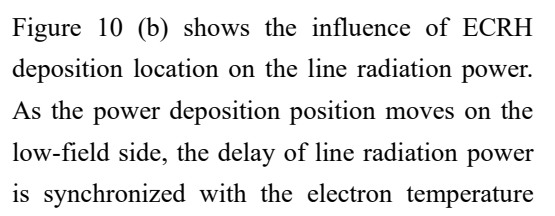
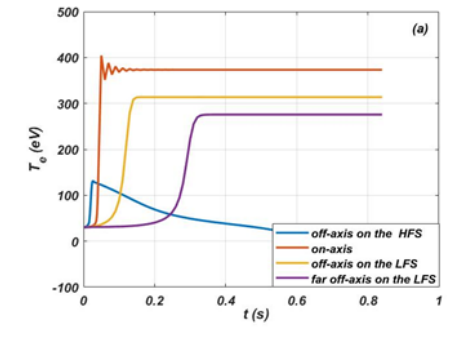


FIG.9 Influence of ECRH power deposition position on power absorption.

shows higher absorption than LFS during the low-density start-up phase (<1×10¹⁸ m⁻³), its efficiency declines rapidly at higher densities due to strong wave refraction, yielding a much lower peak absorption of only 32.39 kW.

Figure 10 (a) shows the effect of ECRH power deposition location on the electron temperature evolution during plasma start-up. When the heating location moves from the low-field side off-axis region toward the on-axis region, the electron temperature rise becomes significantly more rapid, and the electron temperature increases from 275.7 eV to 375 eV. When heating is applied at the high-field side off-axis region, the electron temperature initially increases rapidly but then drops sharply after reaching its peak. However, as the electron density increases, the EC wave begins to be reflected. This reflection reduces the power absorption efficiency, ultimately causing the electron temperature to decline.





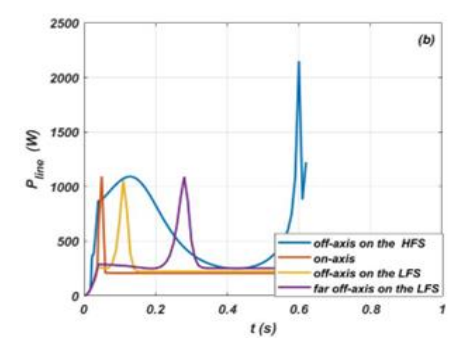


FIG. 10 Effect of ECRH power deposition location on (a) the electron temperature and (b) the line radiation power.

rise and wave power absorption, but the change of power deposition position has no significant effect on the power loss of line radiation power. In conclusion, for the same injection power, on-axis heating causes the electron temperature to rise rapidly and the flat top temperature to be higher, while off-axis heating causes the electron temperature to rise longer and the temperature to be lower. Except for off-axis heating in the high-field side, there is no significant effect on the value of the line radiation power. To facilitate comparison, only the case where on-axis heating is considered in later numerical simulations.

4.4 Effect of impurity concentration on start-up

In this section, the results of the effect of impurity concentration on plasma start-up are given. The iron impurity concentration was scanned over 0.1%, 0.2%, 0.4%, 0.6%, 0.8%, and 1%.

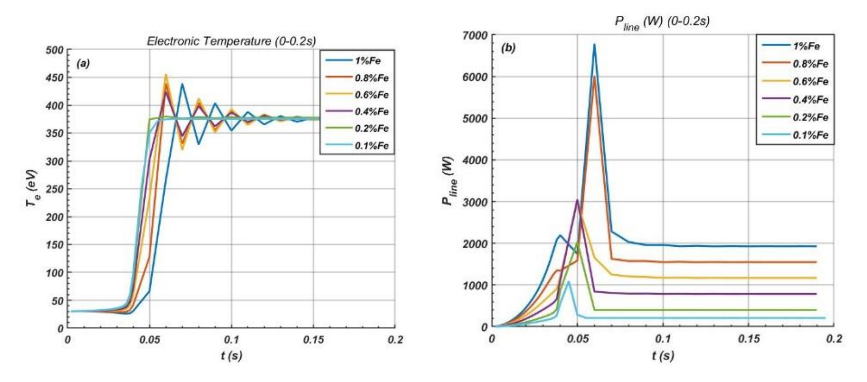


FIG. 11 Effect of iron impurity concentration on (a) the electron temperature within 0.2 s and (b) the line radiation power within 0.2 s.

Figure 11 illustrates these effects within the first 0.2 seconds of the discharge. As the iron impurity concentration increases, the rise in electron temperature becomes slightly delayed. When the iron concentration reaches 0.8%, the peak line radiation power reaches 6 kW. With further increases in iron

concentration, a noticeable drop in electron temperature occurs during the ramp-up phase. Therefore, to maintain effective plasma start-up, the iron impurity concentration should be kept below 0.8%. Under optimal conditions, an initial plasma density of $1\times10^{17}\,\mathrm{m}^{-3}$, ECRH injection power of 200 kW, resonance layer located at the plasma core, and iron impurity concentration of 0.01%—plasma start-up in the CN-H1 stellarator is shown to be feasible.

Figure 12 shows the simulation results of plasma density evolution and EC wave power absorption during ECRH start-up in the CN-H1 stellarator. As the density increases from 1×10^{17} m⁻³ to 2×10^{18} m⁻³, the absorbed EC wave power reaches a maximum of 181 kW, corresponding to an absorption efficiency of up to 94.8%.

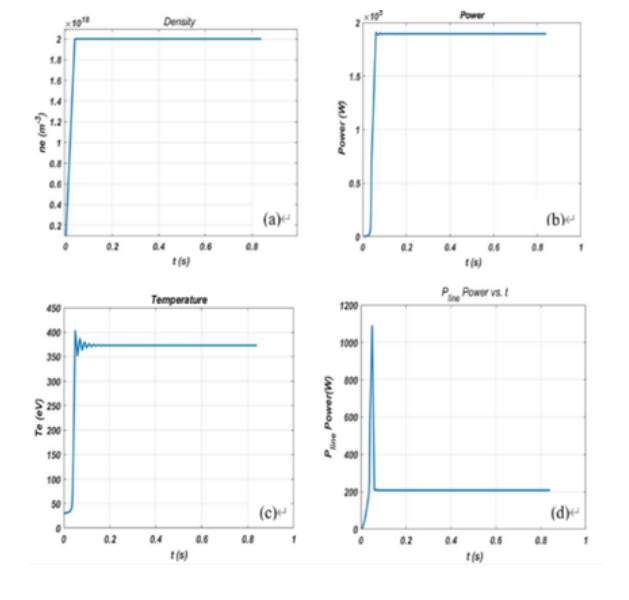


FIG.12 Start-up results for CN-H1 stellarator predicted by the model under 28 GHz ECRH. (a) Temporal evolution of electron density, (b) ECRH power absorption, (c) electron temperature and (d) impuraty line radiation power.

IAEA-CN-316/3225

5. SUMMARY

Based on the energy confinement time scaling law for L-mode plasmas in stellarators, this work establishes a plasma start-up model incorporating the energy balance equation and the equations governing electron cyclotron wave propagation and power deposition in 3D magnetic fields. Under identical plasma parameter conditions, the model is applied to simulate the start-up of the W7-X stellarator. The simulation results are good agreement with experimental observations. Then, this model is utilized to investigate 28 GHz EC wave start-up in the CN-H1 stellarator. A systematic analysis is conducted to examine the effects of the electron-to-ion temperature ratio, injected ECRH power, ECRH power deposition location, and impurity concentrations (iron) on the start-up process.

The research results show that as the T_i/T_e ratio increases, the plateau temperature of the electron temperature rises significantly, indicating that the increase in ion temperature will help the electron temperature reach a higher level. As P_0 increases, both the climbing rate and the plateau temperature of the electron temperature increase. Moreover, when P_0 is greater than 200 kW, the radiative power loss of the plasma is significantly reduced. When the power deposition is on the low-field side and moves from the far-axis to the near-axis region, both the rising rate and the plateau temperature of the electron temperature increase. In addition, the concentrations of iron impurities should be less than 0.8% respectively to ensure the effective startup and heating of the plasma.

In conclusion, under optimized plasma conditions—namely, an ion-to-electron temperature ratio of T_i/T_e = 1, injected ECRH power P_0 = 200 kW with on-axis heating, and impurity concentrations of 0.1% iron—efficient plasma start-up can be achieved. The ECRH power absorption efficiency rapidly increases to 94.8%. When the plasma density reaches 2×10^{18} m⁻³, the electron temperature attains 373.3 eV, and the peak impurity line radiation power is approximately 1.1 kW.

REFERENCES

- [1] PHELANDER. ET AL., PLASMA PHYS. CONTROL. FUSION 54 (2012) 124009
- [2] A.H. BOOZER., J. PLASMA PHYS. 81 (2015) 515810606
- [3] B. D. BLACKWELL. ET AL., AIP CONF. PROC. 669 (2003) 158
- [4] K. NAGASAKI. ET AL., J. PHYS. SOC. JPN. 70 (2001) 617
- [5] SHUANGSHUANG WANG. ET AL., PHYS. SCR. 100 (2025) 025602
- [6] Y. ZHANG. ET AL., NUCL. FUSION 65 (2025) 036041
- [7] YIZHUOHANG LIU. ET AL., PLASMA SCI. TECHNOL. 26 (2024) 075101
- [8] M. ONO. ET AL., PHYS. REV. E 106 (2022) L023201
- [9] M. ONO. ET AL., NUCL. FUSION 62 (2022) 106035
- [10] M. ONO. ET AL., AIP CONF. PROC. 2984 (2023) 110002
- [11] M. ONO. ET AL., NUCL. FUSION 64 (2024) 086021
- [12] M. ONO. ET AL., AIP CONF. PROC. 2254 (2020) 090001
- [13] H.P. LAQUA. ET AL., EPJ WEB CONF. 203 (2019) 02002
- [14] H.P. LAQUA. ET AL., PLASMA FUSION RES.16 (2021) 2402058